

PAPER • OPEN ACCESS

## Local structure determination in helimagnetic $\text{Co}_8\text{Zn}_8\text{Mn}_{4-x}\text{Fe}_x$

To cite this article: D Menzel *et al* 2019 *J. Phys. Commun.* **3** 025001

View the [article online](#) for updates and enhancements.



## PAPER

Local structure determination in helimagnetic  $\text{Co}_8\text{Zn}_8\text{Mn}_{4x}\text{Fe}_x$ 

## OPEN ACCESS

## RECEIVED

19 November 2018

## REVISED

19 December 2018

## ACCEPTED FOR PUBLICATION

24 January 2019

## PUBLISHED

4 February 2019

Original content from this work may be used under the terms of the [Creative Commons Attribution 3.0 licence](#).

Any further distribution of this work must maintain attribution to the author(s) and the title of the work, journal citation and DOI.

D Menzel<sup>1</sup> , D Baabe<sup>2</sup> , FJ Litterst<sup>1</sup> , N Steinki<sup>1</sup> , K Dietze<sup>1</sup> , M Sach<sup>1</sup> , B Rubrecht<sup>1</sup> , S Süllow<sup>1</sup> and A Hoser<sup>3</sup> <sup>1</sup> Institut für Physik der Kondensierten Materie, Technische Universität Braunschweig, D-38106 Braunschweig, Germany<sup>2</sup> Institut für Anorganische und Analytische Chemie, Technische Universität Braunschweig, D-38106 Braunschweig, Germany<sup>3</sup> Helmholtz-Zentrum Berlin für Materialien und Energie, D-14109 Berlin, GermanyE-mail: [d.menzel@tu-braunschweig.de](mailto:d.menzel@tu-braunschweig.de)**Keywords:** local structure, neutron diffraction, SQUID magnetometry, Mössbauer spectroscopy**Abstract**

We have carried out a structural and magnetic characterization of  $\text{Co}_8\text{Zn}_{8+y}\text{Mn}_{4-y-x}\text{Fe}_x$  by means of bulk techniques, powder neutron scattering and Mössbauer spectroscopy. From our data, we derive the main magnetic parameters and carry out a detailed structural characterization. We observe that disorder is present in our samples in various forms and that this seems to be generic for this class of materials. However, the disorder appears to have little impact on the character of the magnetic phases, and thus seems to be of no relevance for the skyrmionic phases established for these types of materials.

**1. Introduction**

In recent years, the field of skyrmionics, i.e. the physics of complex spin textures forming as a result of (local) non-inversion symmetry in magnetic systems, has become the focus of extensive research efforts. A large variety of topics is being studied, with one aspect under investigation the search for new materials that contain skyrmionic phases. There are two fundamentally different approaches to tackle this aspect, the first one aiming to detect bulk magnetic materials which crystallographically lack inversion symmetry [1, 2], the second one utilizing the symmetry breaking at surfaces in thin films [3]. For the first approach, again there are different motifs with respect to the search for new materials—one trying to identify model systems allowing to study fundamental aspects of skyrmion physics, the other attempting to fine-tune material properties that allow skyrmionic phases to exist in technologically relevant temperature and field ranges.

The latter aspect was the starting point for a study on a series of materials with composition  $\text{Co}_{6+x}\text{Zn}_{6+y}\text{Mn}_{8-x-y}$ , with  $x, y \leq 4$  [4, 5]. These systems are derivatives of the binary compound  $\text{Co}_8\text{Zn}_{12}$ , which crystallizes as  $\beta$ -Mn-phase, the corresponding crystallographic unit cell being non-centrosymmetric cubic (space group either  $P4_132$  or  $P4_332$ , lattice parameter  $a \sim 6.35$  Å). The materials undergo magnetic transitions into weakly ferromagnetic or helimagnetic states, and contain in-field regions where magnetic skyrmions form. More specifically, in terms of magnetic order, itinerant ferromagnetism with Curie temperatures up to 460 K was observed for  $\text{Co}_{6+x}\text{Zn}_{6+y}\text{Mn}_{8-x-y}$  [4]. Partial substitution of Cobalt and Zinc with Manganese leads to a significant variation of the Curie temperature and induces helimagnetism causing the stabilization of skyrmionic phases. Notably, for the stoichiometry  $\text{Co}_9\text{Zn}_9\text{Mn}_2$  a metastable skyrmionic phase was identified close to the Curie point even in zero magnetic field [5].

More recently, the sample series became the focus of investigations into more fundamental aspects of skyrmionic behavior. Already the strong dependence of  $T_C$  on the actual stoichiometry observed in [4] indicated significant doping effects. This idea was made more explicit by arguing that replacing Co by a single Fe in  $\text{Co}_{8-x}\text{Fe}_x\text{Zn}_8\text{Mn}_4$  reduces the electron count by one per unit cell [6]. In fact, a significant dependence of  $T_C$  on the composition  $x$  was observed, with  $T_C$  reduced from  $\sim 300$  K at  $x = 0$  to  $\sim 135$  K at  $x = 4.5$ . Moreover, similar to the findings for the B20 compounds [7–12], it was recognized that also the Dzyaloshinskii-Moriya interaction (DMI) causing the formation of skyrmions is a function of band filling, and even changes its sign as function of  $x$ . It implies that for this class of materials the actual stoichiometry is a control parameter for both the overall strength of the magnetic interaction as for the skyrmion formation.

**Table 1.** Room temperature lattice parameters from refinements of the x-ray diffractograms of  $\text{Co}_8\text{Zn}_{8+y}\text{Mn}_{4-y-x}\text{Fe}_x$ .

	$a$ [Å]
$\text{Co}_8\text{Zn}_8\text{Mn}_4$	6.3709(3)
$\text{Co}_8\text{Zn}_8\text{Mn}_{3.5}\text{Fe}_{0.5}$	6.3641(5)
$\text{Co}_8\text{Zn}_8\text{Mn}_3\text{Fe}$	6.3524(6)
$\text{Co}_8\text{Zn}_9\text{Mn}_3$	6.3694(6)

Of course, the argument of band filling can be turned around: For the series of samples  $\text{Co}_8\text{Zn}_8\text{Mn}_{4-x}\text{Fe}_x$  a single Fe adds an electron per unit cell, i.e. changing the Fe content allows material control via site specific doping. As well, naively for an itinerant magnet we would expect that the dependence of the main magnetic parameters should be essentially opposite to that reported in [6]. Only, in this situation it needs to be considered if the specific occupation of the different local sites is of relevance. After all, the class of materials stems from  $\text{Co}_8\text{Zn}_{12}$ , where Co and Zn occupy crystallographic nonequivalent sites. In a neutron-powder-diffraction study of the compound  $\text{Co}_{10}\text{Zn}_{10}$  it has been demonstrated that there is a preferential occupation for the two Wyckhoff positions, with Cobalt on the  $8c$ -sites, and a Zn/Co mixture on the  $12d$ -sites [13]. In doping experiments such as on  $\text{Co}_{8-x}\text{Fe}_x\text{Zn}_8\text{Mn}_4$  or  $\text{Co}_8\text{Zn}_8\text{Mn}_{4-x}\text{Fe}_x$  it is thus of interest to study if the preferential site occupation is retained by the Fe atom, and if it affects relevant magnetic properties. In this situation, we have set out to study  $\text{Co}_8\text{Zn}_8\text{Mn}_{4-x}\text{Fe}_x$ ,  $x \leq 1$ , with respect to its structural properties, and relate these to the main magnetic properties.

In the following, for a series of samples  $\text{Co}_8\text{Zn}_{8+y}\text{Mn}_{4-y-x}\text{Fe}_x$  we will describe sample preparation and the essential characterization of the structural and magnetic properties. Subsequently, we will present a detailed neutron diffraction study aimed at resolving the question of site occupation. Finally, we have carried out an extensive Mössbauer spectroscopy study, which allows a complementary and local view of the structural and magnetic properties.

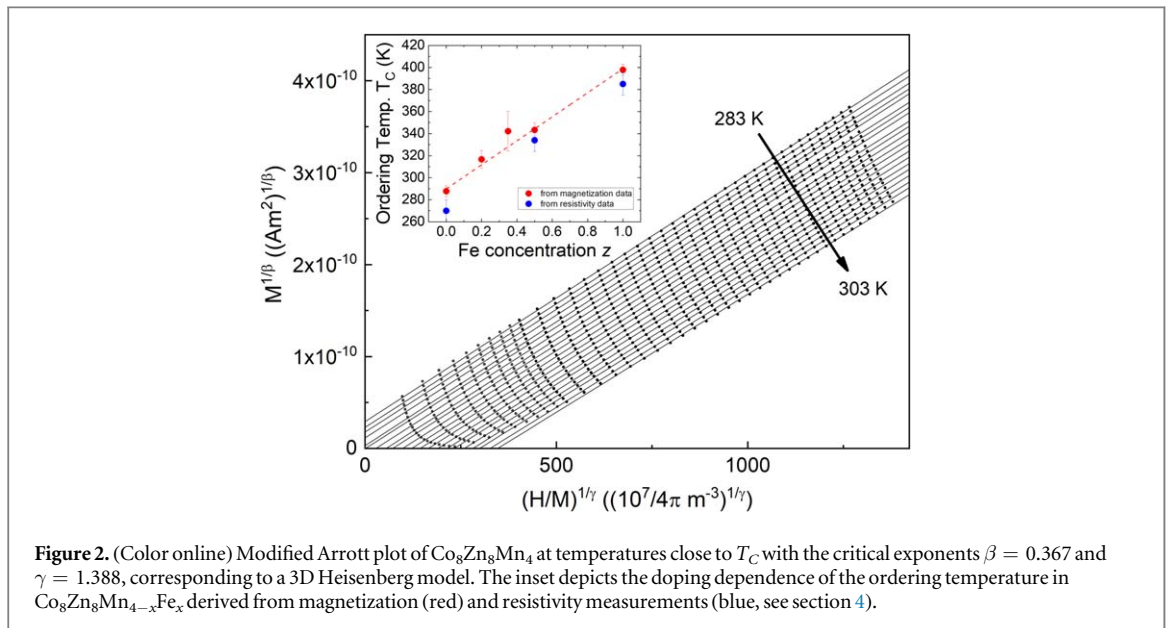
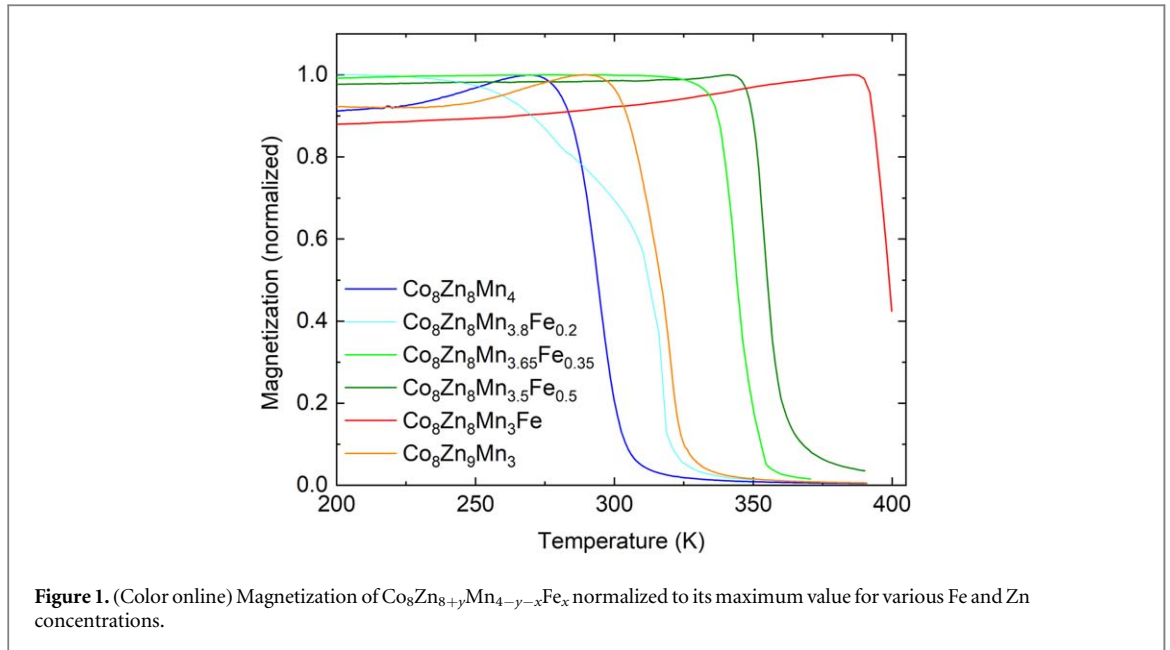
## 2. Sample preparation

Polycrystalline samples of the pseudoternary compound  $\text{Co}_8\text{Zn}_8\text{Mn}_{4-x}\text{Fe}_x$  with  $x = 0, 0.2, 0.35, 0.5$ , and 1 as well as a  $\text{Co}_8\text{Zn}_9\text{Mn}_3$  specimen were synthesized by a thermal reaction similar as described in [13]. Stoichiometric amounts of Co (*Chempur*, 99.95%), Zn (*Koch*, 99.999 8%), Mn (*Chempur*, 99.99%), and Fe (*Alfa Aesar*, 99.98%) were sealed in an evacuated quartz tube ( $p < 10^{-5}$  mbar), heated to 1100°C for 12 hours and cooled down to 925°C with a cooling rate of 1K h<sup>-1</sup>. Subsequently, the polycrystals were annealed at this temperature for 1 week and quenched to room temperature. For Mössbauer spectroscopy measurements we used iron replenished with <sup>57</sup>Fe. All samples tend to be brittle, which has affected the outcome of some of the resistivity measurements.

X-ray powder diffraction shows that all samples crystallize in the  $\beta$ -Mn-phase and, aside from the two samples  $x = 0.2, 0.35$ , are single-phase within experimental resolution. The lattice parameters obtained from the substituted compounds  $\text{Co}_8\text{Zn}_{8+y}\text{Mn}_{4-y-x}\text{Fe}_x$  with  $x, y \leq 1$  are summarized in table 1. They essentially follow Vegard's law [14], ranging from 6.370 9(3)Å for  $\text{Co}_8\text{Zn}_8\text{Mn}_4$  to 6.352 4(6) Å for  $\text{Co}_8\text{Zn}_8\text{Mn}_3\text{Fe}$  at room temperature, in agreement with previous reports [6]. The  $\text{Co}_8\text{Zn}_9\text{Mn}_3$  sample has a lattice parameter consistent with the reports on related compounds.

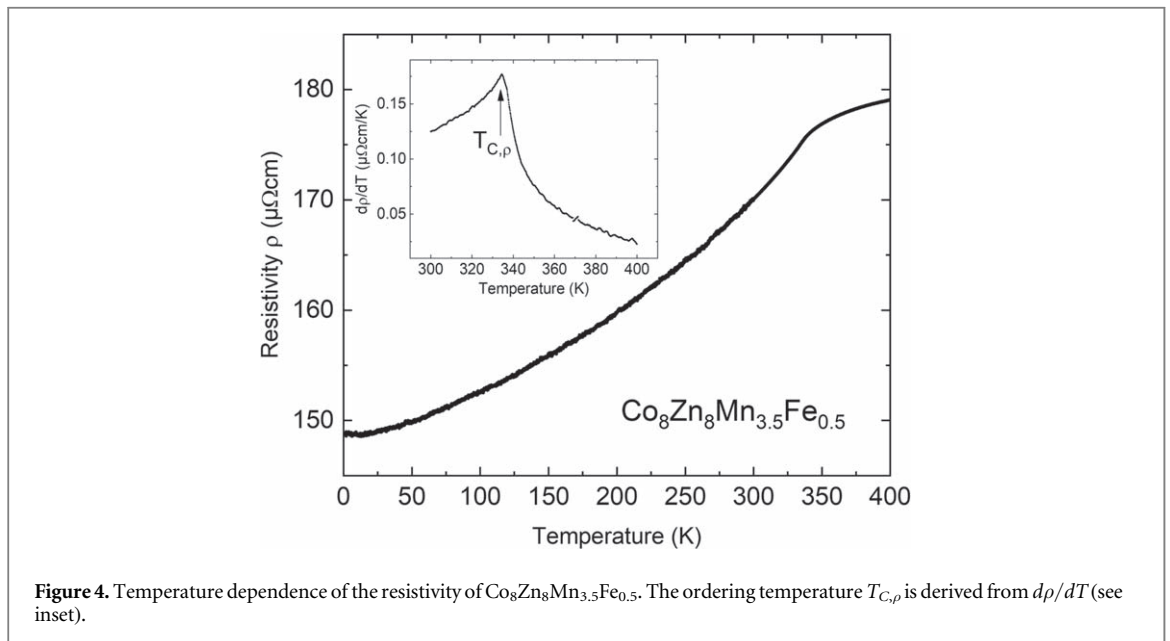
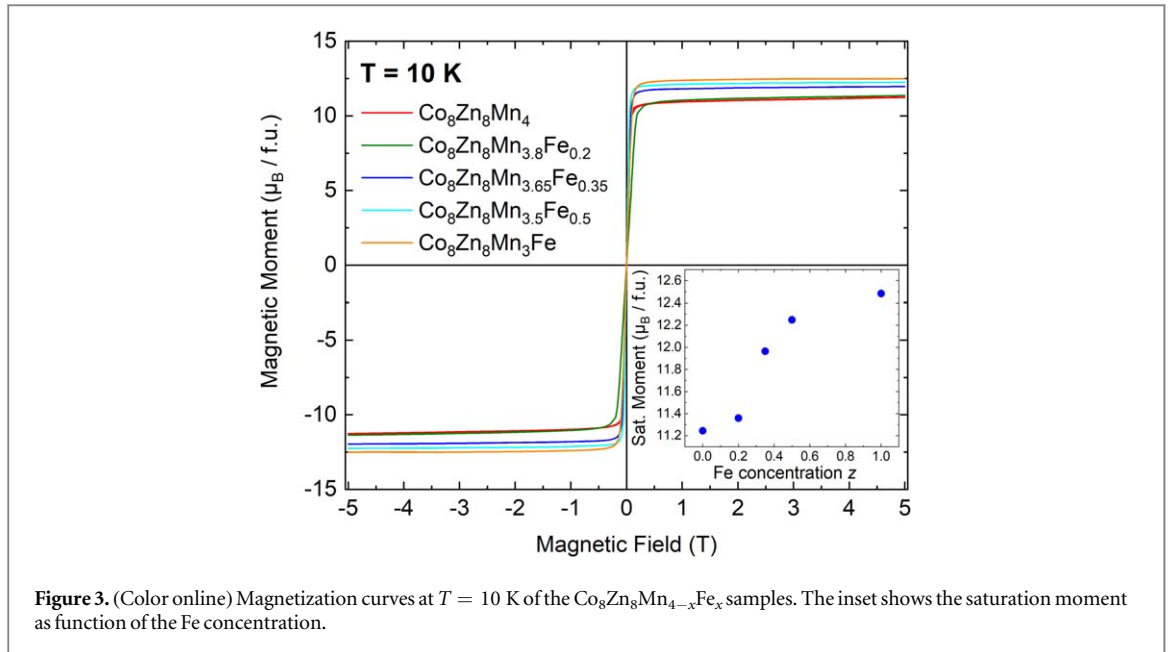
## 3. Magnetic properties

The magnetic characterization of the samples has been carried out in terms of SQUID magnetometry using a *Quantum Design* MPMS-5S system. The magnetization in an external field of 0.01 T has been normalized to the maximum value of the individual sample and is plotted as function of the temperature in figure 1. The ordering temperature  $T_C$  shows a strong dependence on the Fe-concentration and varies between 288 K and 398 K for  $x = 0$  and 1, respectively (see inset of figure 2). This increase of  $T_C$  would be consistent with the band filling argument put forth in [6] to account for the doping dependence in  $\text{Co}_{8-x}\text{Fe}_x\text{Zn}_8\text{Mn}_4$ . Regarding the magnetic susceptibility  $\chi$ , the complete solid solution series  $\text{Co}_8\text{Zn}_8\text{Mn}_{4-x}\text{Fe}_x$  reveals a magnetic behavior very similar to the parent compound  $\text{Co}_8\text{Zn}_8\text{Mn}_4$  and to  $\text{Co}_8\text{Zn}_9\text{Mn}_3$  [4], suggesting that skyrmions are expected to form also for the mixed compounds in an applied magnetic field just below  $T_C$ .



Arrott plots, i.e. the dependence of  $M^2$  versus  $M/H$ , with the magnetization  $M$  and the external field  $H$ , are commonly used to determine the ordering temperature in an accurate way. Moreover, they are able to provide information about the critical behaviour when they are modified such that  $M^{1/\beta}$  is plotted versus  $(H/M)^{1/\gamma}$ . Here,  $\beta$  and  $\gamma$  denote the critical exponents which are defined by  $\chi \propto (T - T_C)^\gamma$  for  $T > T_C$  and  $M \propto (T_C - T)^\beta$  for  $T < T_C$  [15, 16]. As an example, a modified Arrott plot for  $\text{Co}_8\text{Zn}_8\text{Mn}_4$  is shown in figure 2. In the high field regime, parallel straight lines are obtained for  $\beta = 0.367$  and  $\gamma = 1.388$ , consistent with a 3D Heisenberg model. The ordering temperature, which is obtained from the intersect of the straight lines with the origin of the plot, is displayed in the inset of figure 2 for the compounds  $\text{Co}_8\text{Zn}_8\text{Mn}_{4-x}\text{Fe}_x$ , closely following the results of the susceptibility measurements (cf figure 1).

Magnetization curves taken at  $T = 10$  K show a soft magnetic behaviour of  $\text{Co}_8\text{Zn}_8\text{Mn}_{4-x}\text{Fe}_x$  with a coercivity  $< 1$  mT (figure 3). Upon Fe doping, the saturation magnetization increases by  $\approx 1 \mu_B$  from  $11.3$  to  $12.4 \mu_B/\text{f.u.}$ , which is usual for a 3D Heisenberg-type itinerant magnet.



#### 4. Resistivity

Transport measurements have been performed below 300 K in a  $^4\text{He}$  Oxford cryostat and for high temperatures inside a resistively heated oven. The samples were cut into  $10\text{ mm} \times 1\text{ mm} \times 1\text{ mm}$  bars and contacted using silver glue for a four-terminal measurement. As an example, in figure 4 the resistivity is shown for the  $\text{Co}_8\text{Zn}_8\text{Mn}_{3.5}\text{Fe}_{0.5}$  specimen.

The resistivity of all samples shows a metallic behavior, even if the absolute values of more than one hundred  $\mu\Omega\text{cm}$  are quite high. The residual resistivity ratio  $\rho_{300\text{K}}/\rho_{T \rightarrow 0}$  is small and does not exceed 1.20 for the different samples. These findings indicate the presence of a high degree of structural disorder and/or micro-sized cracks throughout the samples, which leads to enhanced scattering and extensions of the current path. Still, the transport measurements reflect the transition into magnetically ordered states ( $T_{C,\rho}$ ) at temperatures in accordance with the magnetic susceptibility data by kinks in the resistivity similar to for instance Ni [17]. Although  $T_{C,\rho}$  is due to sample inhomogeneities  $\approx 5\%$  smaller than  $T_C$  from magnetization data, it clearly reproduces the trend of increasing ordering temperature with larger Fe concentration (see inset of figure 2).

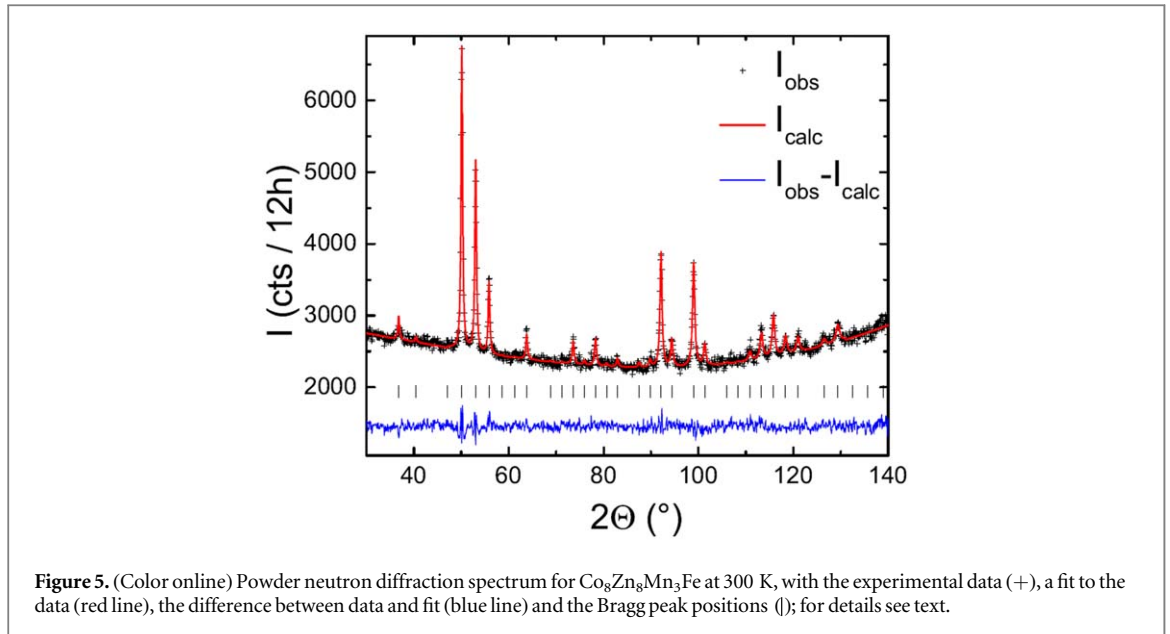


**Figure 5.** (Color online) Powder neutron diffraction spectrum for  $\text{Co}_8\text{Zn}_8\text{Mn}_3\text{Fe}$  at 300 K, with the experimental data (+), a fit to the data (red line), the difference between data and fit (blue line) and the Bragg peak positions (|); for details see text.

## 5. Neutron diffraction

In bulk material, skyrmions are stabilized by the Dzyaloshinskii-Moriya-interaction, which (in a picture of local moments) for neighboring spins  $S_i, S_j$  produces an exchange term  $H \propto S_i \times S_j$  not equal to zero for non-centrosymmetric symmetries. Conversely, a randomized site occupation (as on the  $12d$  site in  $\text{Co}_{10}\text{Zn}_{10}$ ) should be detrimental to skyrmion formation, as it randomizes this exchange. Hence, for a detailed understanding of skyrmions in compound series such as  $\text{Co}_{6+x}\text{Zn}_{6+y}\text{Mn}_{8-x-y}$  or  $\text{Co}_8\text{Zn}_{8+y}\text{Mn}_{4-y-x}\text{Fe}_x$  it is important to determine the actual site occupation.

Suggested by [13], for  $\text{Co}_8\text{Zn}_8\text{Mn}_4$  we expect Co to occupy the  $8c$  sites, while Zn and Mn sit on the  $12d$  sites. For Fe doping, conceptually, in the present case, three scenarios appear possible, that is Fe exclusively occupies either the  $12d$  or  $8c$  sites (i.e. weak disorder), or it is (evenly) distributed on all positions (strong disorder). With their similar atomic numbers, for the  $3d$  transition metals Co, Zn, Mn and Fe a determination of the elemental site occupation by means of x-ray powder diffraction is not attainable. Instead, as has been demonstrated in the [13, 18], neutron powder diffraction provides a much brighter elemental contrast and thus allows to determine the elemental occupation of the distinct crystallographic sites. Therefore, we have carried out a neutron scattering investigation using the Fine Resolution Powder Diffractometer E9 of the BENSCH, Helmholtz-Center Berlin, to structurally characterize two materials out of the series  $\text{Co}_8\text{Zn}_8\text{Mn}_{4-x}\text{Fe}_x$ , that is  $\text{Co}_8\text{Zn}_8\text{Mn}_3\text{Fe}$  and  $\text{Co}_8\text{Zn}_8\text{Mn}_{3.5}\text{Fe}_{0.5}$ .

Experiments have been carried out in zero field, with one run each for a temperature above/below  $T_C$ , that is at 300 and 440 K. A neutron wavelength of  $\lambda = 1.7982 \text{ \AA}$  has been used. In the figures 5 and 6 we plot the experimental data at 300 K for  $\text{Co}_8\text{Zn}_8\text{Mn}_3\text{Fe}$  and  $\text{Co}_8\text{Zn}_8\text{Mn}_{3.5}\text{Fe}_{0.5}$ , here including fits of the data (see discussion below). Regarding the raw data, first and foremost, the very large background scattering is remarkable (background of about 1500 up to 3000 counts, as compared to a maximum Bragg peak with about 4000 counts). This observation suggests that there is a substantial amount of amorphicity or structural short range order in our samples. Since our sample series overall exhibits a behavior similar to that reported for instance in [4], we suspect that this trend to structural disorder is inherent to polycrystalline specimens of this sample class.

Starting with the data for  $\text{Co}_8\text{Zn}_8\text{Mn}_3\text{Fe}$ , from a comparison of the scans above and below  $T_C$  we find no intensity that we could associate to magnetic scattering. This is not unexpected, as a helimagnetic scattering component will produce intensity mostly at very low angles (see SANS experiments in the [4–6]). Moreover, with the large experimental background any residual signal in the scan from magnetic order in our experimental angular window is probably hidden by the experimental noise. In result, we can proceed and analyze the data just assuming a structural scattering component.

On top of the large background, we observe a well-defined scattering spectrum that can be ascribed to the  $\beta$ -Mn-structure (see below). The Bragg peaks themselves do not appear broadened, which implies that our sample should be considered as consisting of reasonably crystalline and extended spatial areas  $\text{Co}_8\text{Zn}_8\text{Mn}_3\text{Fe}$ , which are separated by comparatively wide amorphous or short range ordered grain boundaries.

Taking account of the background using a polynomial spline, we can fit the Bragg peak spectrum of  $\text{Co}_8\text{Zn}_8\text{Mn}_3\text{Fe}$  using the  $\beta$ -Mn-structure, as demonstrated by the matching of the expected Bragg peak positions

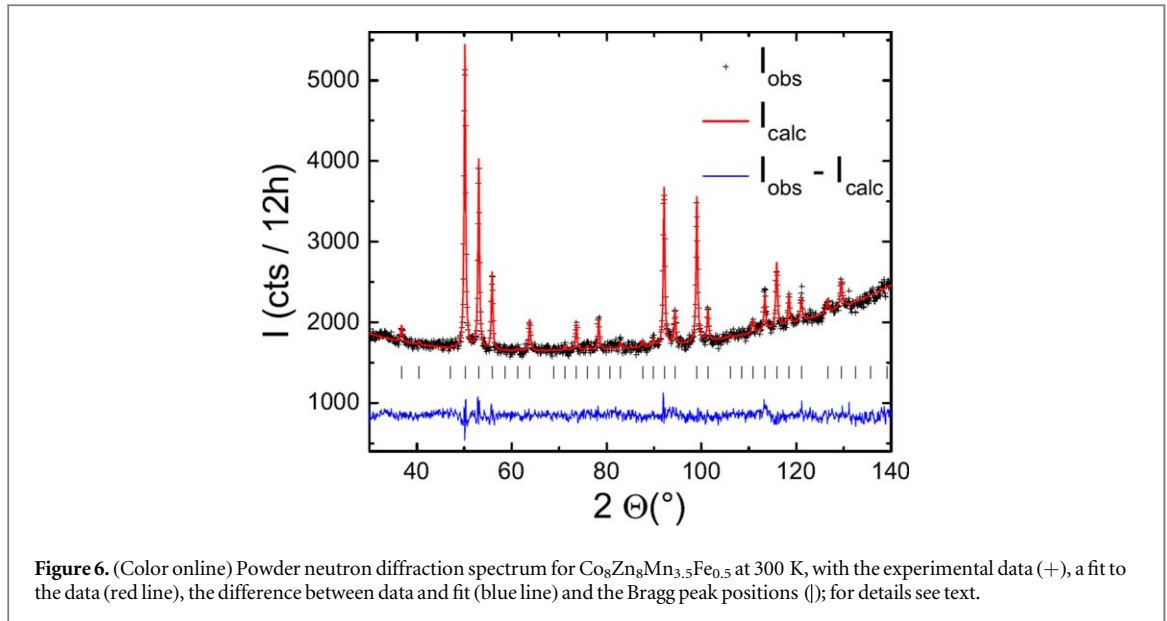


**Figure 6.** (Color online) Powder neutron diffraction spectrum for  $\text{Co}_8\text{Zn}_8\text{Mn}_{3.5}\text{Fe}_{0.5}$  at 300 K, with the experimental data (+), a fit to the data (red line), the difference between data and fit (blue line) and the Bragg peak positions (|); for details see text.

**Table 2.** Fit parameters of refinements of the neutron powder diffractograms of  $\text{Co}_8\text{Zn}_8\text{Mn}_{4-x}\text{Fe}_x$  assuming nominal composition.

$x$	1	1	0.5	0.5
$T$ (K)	440	300	440	300
$a$ [ $\text{\AA}$ ]	6.3681(3)	6.3512(3)	6.3778(4)	6.3661(2)
$x_{12d}$	0.7963(6)	0.7976(6)	0.7995(6)	0.7970(5)
$y_{12d}$	0.0463(6)	0.0476(6)	0.0495(6)	0.0470(5)
$z_{12d}$	0.125	0.125	0.125	0.125
$B_{\text{iso}-12d}$	2.1(2)	2.1(2)	1.4(2)	1.4(1)
$x_{8c}$	0.9320(8)	0.9325(8)	0.9355(8)	0.9317(7)
$y_{8c}$	0.43120(8)	0.4325(8)	0.4355(8)	0.4317(7)
$z_{8c}$	0.0680(8)	0.0675(8)	0.0645(8)	0.0683(7)
$B_{\text{iso}-8c}$	0.1(1)	0.2(1)	0.1	0.4(1)
$R_{\text{Bragg}}$	10.4%	6.3%	18.1%	9.3%
$\chi^2$	1.10	0.95	2.02	1.01

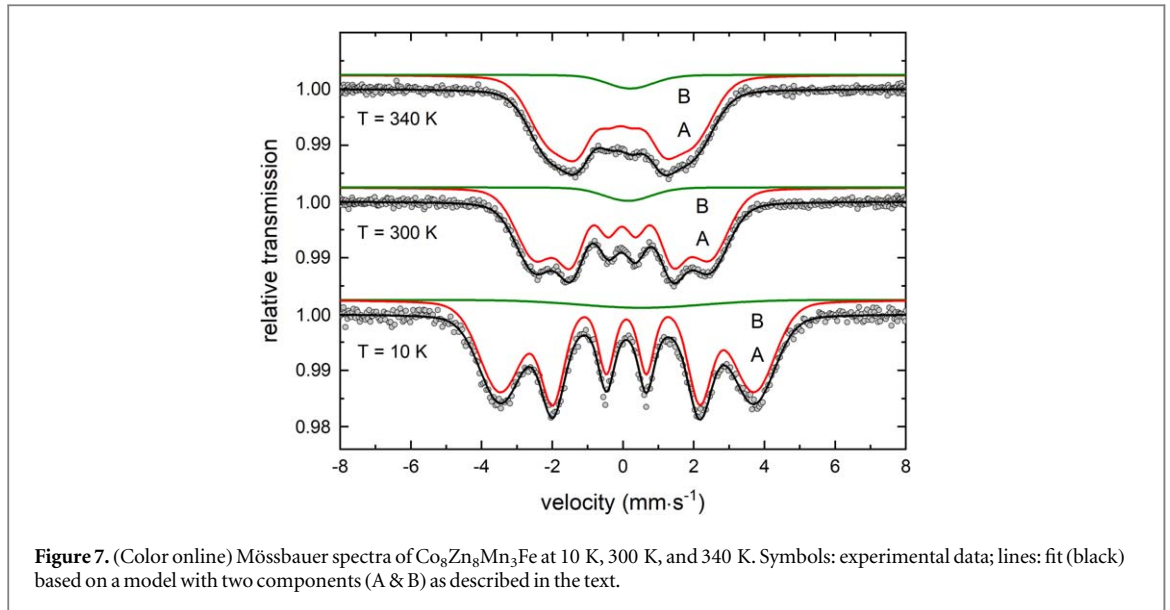
with the observed ones (see figure 5). In fact, in our experimental data there is not a single Bragg peak that is not accounted for by the  $\beta$ -Mn-phase, reflecting the absence of a significant amount of secondary phases. A summary of the structural parameters obtained from our fits is given in table 2.

As a next step, we can now study the site occupation by fitting with different structural models. We start out with the ‘weak disorder’ model of Fe residing entirely on the 12d sites. From our fit, and using the nominal composition of our sample, we can nicely describe the experimental data (red line in figure 5 as an example for 300 K data; the difference between data and fit is included in the plot as blue line, shifted for clarity). For the 440 K data (not shown), from the fit we attain a refinement value of  $R_{\text{Bragg}} = 10.4\%$ , with about half of the  $R_{\text{Bragg}}$  stemming from the scatter of the background.

Allowing for a deviation from nominal stoichiometry, but staying with the ‘weak-disorder’ model of Fe on the 12d-site, it leads to an optimal solution for a composition  $\text{Co}_8\text{Zn}_{7.78}\text{Mn}_{2.96}\text{Fe}_{0.93}$  with a slightly reduced  $R_{\text{Bragg}} = 9.7\%$ . Given the large experimental background, we conclude that within experimental error there is no difference between nominal and fitted optimum composition.

Conversely, if we assume that Fe partially resides on the 8c-sites, we find a continuous degradation of the fit quality. Ultimately, for Fe only occupying 8c, the refinement yields a value  $R_{\text{Bragg}} = 20\%$ , with a clear mismatch of intensity for various Bragg peaks. We thus conclude that in  $\text{Co}_8\text{Zn}_8\text{Mn}_3\text{Fe}$  the Fe ion entirely occupies the 12d-sites, together with Mn and Zn, while Co occupies the 8c-site. Comparing our fit result with previous reports (see [13]), we find good agreement regarding atomic coordinates. The rather large  $B_{\text{iso}}$  values of the 12d sites suggest some strain disorder on this site, likely as result of the doping [19].

Subsequently, we have performed a similar analysis for the data taken at 300 K, i.e. below  $T_C \sim 400$  K. The fitting produces similar refinement results with an even better matching between calculation and experiment,



and lattice parameters that are close to the values previously reported for samples  $\text{Co}_{6+x}\text{Zn}_{6+y}\text{Mn}_{8-x-y}$  and from our x-ray diffraction experiments.

The procedure described so far has equally been applied to the data taken for the sample  $\text{Co}_8\text{Zn}_8\text{Mn}_{3.5}\text{Fe}_{0.5}$ . As illustration, in figure 6 we plot the corresponding data and fits for the measurement carried out at 300 K, while in the table 2 we summarize the corresponding parameters for both temperatures. Again, using the nominal composition a decent fit of the data can be obtained. Conversely, using the occupational numbers as fitting parameters, in this case we cannot improve the fitting, as measured by  $R_{\text{Bragg}}$ . As before, allowing Fe to occupy the 8c reduces the quality of the fit significantly ( $R_{\text{Bragg}} = 13.5\%$  for Fe only on 8c for the 300 K data).

## 6. Zero-field $^{57}\text{Fe}$ Mössbauer spectroscopy

To further investigate the magnetic properties discussed above, supplementary Mössbauer spectroscopic measurements were performed on a standard transmission spectrometer with sinusoidal velocity sweep. While SQUID magnetometry reveals integral magnetic properties of the samples, Mössbauer spectroscopy provides a local probe technique, which allows to study the local magnetic environment at the  $^{57}\text{Fe}$  nucleus site. However, since a very low  $^{57}\text{Fe}$  content of  $\approx 0.11\%$  is present in  $\text{Co}_8\text{Zn}_8\text{Mn}_3\text{Fe}$  with natural isotopic distribution, we prepared a  $^{57}\text{Fe}$ -enriched sample in which  $\approx 20\%$  of the iron atoms of the compound were replenished with the isotope  $^{57}\text{Fe}$  (providing a 10-times larger  $^{57}\text{Fe}$  content of  $\approx 1\%$ ). The measurements on this sample were conducted at temperatures between  $T = 10$  and 340 K and, exemplarily, spectra at  $T = 10, 300$  and 340 K are shown in figure 7.

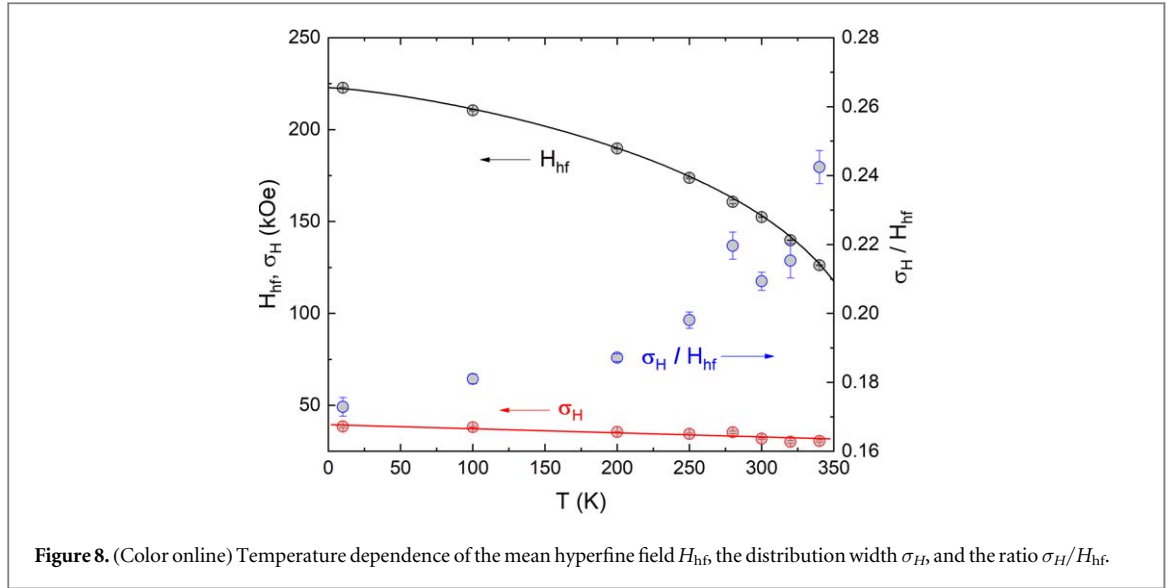
Below  $T \approx 300$  K, the obtained spectra show a resolved hyperfine magnetic sextet (spectrum ‘A’ in figure 7), albeit the line-shape and large line-widths are indicative for the presence of a distribution of hyperfine interactions. Origins can be either (i) a distribution of different chemical  $^{57}\text{Fe}$  environments due to a statistical site occupation of  $^{57}\text{Fe}$  on the available sites in the crystal lattice and/or due to varying numbers of Zn and Mn on nearest neighbor sites leading to a distribution of isomer shifts and hyperfine magnetic fields, or (ii) a distribution of exchange coupling strengths that predominantly vary the local hyperfine magnetic fields at different Fe sites. From the visibly larger broadening of the outer versus the inner spectral lines we conclude that the broadening is dominantly caused by a distribution of magnetic hyperfine fields  $H_{\text{hf}}$ . For fitting the experimental data we, therefore, used a model assuming a Gaussian-shaped distribution of magnetic hyperfine fields and, in addition, for each magnetic hyperfine field a distribution of isomer shifts  $\delta$  with widths  $\sigma_H$  or  $\sigma_\delta$ , respectively. Notably, a neglect of the distribution of isomer shifts gave unsatisfying fit results.

The parameters finally determined on basis of this model are summarized in table 3. Furthermore, since the results of neutron diffraction experiments described above revealed significant contributions of incoherent scattering, this motivated us to consider thus a second component to simulate the experimental Mössbauer spectra. The use of this additional component (spectrum ‘B’ in figure 7) significantly improves the quality of the fit and resulted in a single line component with large values for the line width reflected in a wide distribution  $\sigma_\delta$ . Its temperature dependence points to magnetic origin and we interpret it to be caused by a strongly reduced and widely distributed hyperfine magnetic field. We relate these iron sites to an amorphous magnetic phase in



**Table 3.** Parameters determined on base of the model described in the text.  $\sigma_{\delta,H}$  and  $\Gamma$  describe the distribution widths and Lorentzian line widths (FWHM), respectively.  $\Gamma$  was determined at  $T = 10$  K revealing a value close to the standard experimental line width of the spectrometer of approx.  $0.24 \text{ mm s}^{-1}$ . The hyperfine field  $H_{\text{hf}}$  and the isomer shift  $\delta$  are mean values, the latter of which is quoted relative to  $\alpha$ -Fe at ambient temperature and is not corrected in terms of the second order Doppler effect; (\*) fixed in the fit.

$T$ (K)	$\delta$ ( $\text{mm s}^{-1}$ )	$\sigma_{\delta}$ ( $\text{mm s}^{-1}$ )	$\Delta E_Q$ ( $\text{mm s}^{-1}$ )	$H_{\text{hf}}$ (kOe)	$\sigma_H$ (kOe)	$\Gamma$ ( $\text{mm s}^{-1}$ )	area (%)
10	0.221(4)	0.37(2)	0.024(7)	222.7(4)	38.5(6)	0.29(3)	94*
	0.65(20)	1.28(7)	0*	0*	0*		6*
100	0.29*	0.207(3)	0.35(1)	0.017(6)	210.5(3)	38.1(3)	
	0.38(8)	0.96(3)	0*	0*	0*		6*
200	0.29*	0.158(2)	0.36(1)	0.015(4)	189.7(2)	35.5(2)	
	0.41(4)	0.90(2)	0*	0*	0*		6*
250	0.29*	0.122(5)	0.37(1)	0.014(7)	173.7(4)	34.4(4)	
	0.23(29)	1.09(90)	0*	0*	0*		6*
280	0.29*	0.096(6)	0.36(1)	0.001(9)	160.7(9)	35.3(6)	
	0.14(6)	0.79(4)	0*	0*	0*		6*
300	0.29*	0.095(7)	0.46(1)	0.006 (10)	152.4(1)	31.9(4)	
	0.26(4)	0.78(2)	0*	0*	0*		6*
320	0.29*	0.082(5)	0.51(1)	0.002(5)	139.8(2)	30.1(7)	
	0.38(6)	0.77(4)	0*	0*	0*		6*
340	0.29*	0.050(7)	0.51(1)	0.013 (10)	126.2(3)	30.6(6)	
	0.21(4)	0.75(2)	0*	0*	0*		6*



$\text{Co}_8\text{Zn}_8\text{Mn}_3\text{Fe}$ . The volume fraction of this component lies between 4 and 8% depending on the temperature. Since no systematical change with temperature was observed, we fixed this value in the fit to an average value of 6%.

The analysis of the main component (>90%) of the Mössbauer spectra of  $\text{Co}_8\text{Zn}_8\text{Mn}_3\text{Fe}$  showed values for the isomer shift  $\delta$  increased by about  $0.1 \text{ mm s}^{-1}$  against those of metallic iron indicating a reduced  $s$ -electron charge density at iron in our compound. The temperature dependence of  $\delta$  is small and can be attributed predominantly to the second-order Doppler effect [20]. The distribution width of the isomer shift  $\sigma_\delta$  is relatively wide and can be related with varying local  $s$ -electron densities at Fe due to changing numbers of Zn and Mn nearest neighbor atoms. A more detailed interpretation aiming to a correlation between magnetic hyperfine fields and isomer shifts is yet precluded due to the dominant broadening caused by the magnetic hyperfine splitting.

The values determined for the quadrupole splitting  $\Delta E_Q$  are also virtually temperature independent and close to  $\Delta E_Q = 0$ . Despite cubic symmetry one may expect some electric field gradient at the iron sites due to chemical disorder within the cubic unit cell. From the widely distributed angle between electric field gradient axes and magnetic hyperfine field in a helimagnet this is expected to be averaged to an only small value as observed in our spectra. A more detailed analysis would require measurements in the paramagnetic range above  $T_C$  where the magnetic hyperfine field is vanishing. Yet, this is precluded by the limitation of our installation to lower temperatures.

The magnetic hyperfine field saturates at low temperatures with about 223 kOe, a value clearly reduced compared to metallic iron what can be related to a reduction of  $s$ -electron spin density at iron, which goes in parallel to the observed increase of isomer shift. We relate this to be mainly due to the presence of Zn in the direct neighborhood of Fe. E.g., both increased isomer shifts and reduced hyperfine magnetic fields have been reported for amorphous Fe alloys upon increasing Zn-content [21].

For describing the temperature dependent magnetic hyperfine field  $H_{\text{hf}}$  reflecting the local magnetization we used the function

$$H_{\text{hf}} = H_0 \left( 1 - \left[ \frac{T}{T_C} \right]^\beta \right)^\gamma \quad (1)$$

A free fit resulted in parameters  $\beta = 0.29(2)$ ,  $\gamma = 1.33(9)$ . These values are in good accord with our analysis of magnetization using the modified Arrott and support a Heisenberg model for 3D systems [22]. The extrapolated ordering temperature  $T_C = 382(5) \text{ K}$  is also in good agreement with  $T_C = 397 \text{ K}$  observed for  $\text{Co}_8\text{Zn}_8\text{Mn}_3\text{Fe}$  in the SQUID data.

From the ratio of the distribution width  $\sigma_H$  and the hyperfine field  $H_{\text{hf}}$  one can estimate the thermal evolution of the exchange interaction and the saturation moment of the Fe. The fit results of the Mössbauer spectra (table 3) reveal that  $\sigma_H/H_{\text{hf}}$  increases towards the ordering temperature whereas it changes only slightly between 10 and  $\approx 200 \text{ K}$  (figure 8). We conclude that the temperature dependence of  $\sigma_H/H_{\text{hf}}$  is dominated by variations of the exchange interactions induced by statistical  $^{57}\text{Fe}$  site occupation. This is also reflected in the phase transition observed in the transport measurements which is considerably smeared out.

## 7. Discussion and conclusion

Summarizing, we have performed a detailed study on the doping dependence of the structural and magnetic properties of polycrystalline  $\text{Co}_8\text{Zn}_8\text{Mn}_4$ . From our global characterization of the magnetic properties, we find a behavior similar to that reported for closely related compounds [4–6], suggesting a helical magnetic ground state for all our systems. Following the arguments set out in [6], the dependence of the magnetic transition temperature on Fe doping on the Mn site likely can be understood as band filling effect.



The electronic transport properties of our samples are already indicative of heavily disordered material. This notion is proven by our structural characterization by means of neutron scattering and Mössbauer spectroscopy. According to these measurements, we conclude that there are various types of disorder in our samples  $\text{Co}_8\text{Zn}_8\text{Mn}_{4-x}\text{Fe}_x$ . The large background observed in both neutron scattering and Mössbauer spectroscopy, together with the existence of spectral components from extended crystalline areas, suggest that our materials consist of crystalline grains embedded in a heavily disordered (amorphous or short-range ordered) matrix. From the Mössbauer experiments we assess the volume fraction of disordered material to about 6%, while the absence of a line broadening in the neutron scattering experiments puts a lower limit of a few hundred Å to the crystal grain size. With respect to the structural quality of the crystalline grains, the rather large  $B_{\text{iso}}$  values of the 12d sites and the broadened Mössbauer lines suggest some disorder on this site as well.

While we thus have established a significant degree of disorder in our samples  $\text{Co}_8\text{Zn}_8\text{Mn}_{4-x}\text{Fe}_x$ , it appears not to affect the magnetic properties in a significant way. Qualitatively, it likely reflects the itinerant nature of magnetic order in this class of materials, together with the long-range modulated magnetic structures in the helical/skymionic phases. In this situation, local distortions apparently do not heavily affect the overall magnetic properties. Correspondingly, it appears possible to include all disorder effects as a statistical average, as it has been done for instance for  $\text{Mn}_{1-x}\text{Fe}_x\text{Ge}$  [23]. Conversely, of course, it raises the question if in case of much shorter characteristic length scales of the modulated magnetic structures the effect of crystallographic disorder will be much more pronounced.

## Acknowledgments

We thank the Helmholtz-Zentrum Berlin for the allocation of neutron radiation beamtime. We gratefully acknowledge support by the Braunschweig International Graduate School of Metrology B-IGSM and the DFG Research Training Group GrK 1952/1 Metrology for Complex Nanosystems. We furthermore acknowledge support by the German Research Foundation and the Open Access Publication Funds of the Technische Universität Braunschweig.

## ORCID iDs

D Menzel  <https://orcid.org/0000-0001-6455-3868>  
D Baabe  <https://orcid.org/0000-0001-6931-4866>  
FJ Litterst  <https://orcid.org/0000-0002-5026-5563>  
N Steinki  <https://orcid.org/0000-0003-1274-1781>  
K Dietze  <https://orcid.org/0000-0002-1208-2723>  
M Sach  <https://orcid.org/0000-0003-2909-6539>  
B Rubrecht  <https://orcid.org/0000-0002-2214-5564>  
S Süllow  <https://orcid.org/0000-0001-8522-1360>  
A Hoser  <https://orcid.org/0000-0002-1581-749X>

## References

- [1] Mühlbauer S, Binz B, Jonietz F, Pfleiderer C, Rosch A, Neubauer A, Georgii R and Böni P 2009 *Science* **323** 915
- [2] Yu X Z, Kanazawa N, Onose Y, Kimoto K, Zhang W Z, Ishiwata S, Matsui Y and Tokura Y 2011 *Nat. Mater.* **10** 106
- [3] Heinze S, von Bergmann K, Menzel M, Brede J, Kubetzka A, Wiesendanger R, Bihlmayer G and Blügel S 2011 *Nat. Phys.* **7** 713
- [4] Tokunaga Y, Yu X Z, White J S, Rønnow H M, Morikawa D, Taguchi Y and Tokura Y 2015 *Nat. Comm.* **6** 7638
- [5] Karube K, White J S, Morikawa D, Bartkowiak M, Kikkawa A, Tokunaga Y, Arima T, Rønnow H M, Tokura Y and Taguchi Y 2017 *Phys. Rev. Materials* **1** 074405
- [6] Karube K et al 2018 *Phys. Rev. B* **98** 155120
- [7] Grigoriev S V et al 2010 *Phys. Rev. B* **81** 012408
- [8] Grigoriev S V, Chernyshov D, Dyadkin V A, Dmitriev V, Maleyev S V, Moskvina E V, Menzel D, Schoenes J and Eckerlebe H 2009 *Phys. Rev. Lett.* **102** 037204
- [9] Morikawa D, Shibata K, Kanazawa N, Yu X Z and Tokura Y 2013 *Phys. Rev. B* **88** 024408
- [10] Grigoriev S V et al 2013 *Phys. Rev. Lett.* **110** 207201

- [11] Shibata K, Yu X Z, Hara T, Morikawa D, Kanazawa N, Kimoto K, Ishiwata S, Matsui Y and Tokura Y 2013 *Nat. Nanotechnol* **8** 723
- [12] Grigoriev S V et al 2014 *Phys. Rev. B* **90** 174414
- [13] Xie W, Thimmaiah S, Lamsal J, Liu J, Heitmann T W, Quirinale D, Goldman A I, Pecharsky V and Miller G J 2013 *Inorg. Chem.* **52** 9399
- [14] Vegard L 1921 *Zeitschrift für Physik* **5** 17
- [15] Fisher M E 1967 *Rep. Prog. Phys.* **30** 615
- [16] Stanley H E 1971 *Introduction to Phase Transitions and Critical Phenomena* (London: Oxford University Press)
- [17] Craig P P, Goldberg W I, Kitchens T A and Budnick J I 1967 *Phys. Rev. Lett.* **19** 1334
- [18] Maksimov I, Baabe D, Klauss H H, Litterst F J, Feyerherm R, Többens D M, Matsushita A and Süllo S 2001 *J. Phys.: Condens. Matter* **13** 5487
- [19] Süllo S, Otop A, Loose A, Klenke J, Prokhnenko O, Feyerherm R, Hendrikx R W A, Mydosh J A and Amitsuka H 2008 *J. Phys. Soc. Jpn.* **77** 024708
- [20] Wegener H 1965 *Der Mössbauereffekt und seine Anwendung in Physik und Chemie* (Mannheim: Bibliographisches Institut)
- [21] Laggoun A, Hauet A and Teillet J 1990 *Hyperfine Interact* **54** 825
- [22] Nolting W and Ramakanth A 2009 *Quantum Theory of Magnetism* (Berlin, Heidelberg: Springer)
- [23] Gayles J, Freimuth F, Schena T, Lani G, Mavropoulos P, Duine R A, Blügel S, Sinova J and Mokrousov Y 2015 *Phys. Rev. Lett.* **115** 036602